ELSEVIER

Biophysical Chemistry 108 (2004) 77–87

Biophysical Chemistry

www.elsevier.com/locate/bpc

Re-examining the oligomerization state of macrophage migration inhibitory factor (MIF) in solution

John S. Philo[a,*], Tzung-Horng Yang[b], Michael LaBarre[b]

[a]*Alliance Protein Laboratories, 3957 Corte Cancion, Thousand Oaks, CA 91360, USA*
[b]*IDEC Pharmaceuticals, 3010 Science Park Road, San Diego, CA 92191, USA*

Abstract

The state of oligomerization of macrophage migration inhibitory factor (MIF, also known as glycosylation inhibiting factor, GIF) in solution has been variously reported as monomer, dimer, trimer, or mixtures of all three. Several crystal structures show MIF to be a trimer. Sedimentation velocity shows a recombinant human MIF sample is quite homogeneous, with 98% as a species with $s_{20,w}=3.07$ S and $D_{20,w}=8.29\times10^{-7}$ cm^2/s. Using the partial specific volume calculated from the amino acid composition these values imply a mass of 33.56 kDa, well above that of dimer, but also 9% below the trimer mass of 37.035 kDa. Sedimentation equilibrium data at loading concentrations from 0.01 to 1 mg/ml show unequivocally that the self-association is extremely tight. However, the apparent mass is 33.53 kDa [95% confidence 33.25–33.82], again 9% below that expected for 100% trimer. To examine the possibility this protein has an unusual partial specific volume, sedimentation equilibrium was also done in H_2O/D_2O mixtures, giving 0.765 ± 0.017 ml/g rather than the calculated 0.735 ml/g. With this revised partial specific volume, the equilibrium and velocity data each give $M=37.9\pm2.8$ kDa, fully consistent with a strongly-associated trimeric quaternary structure.

Keywords: Macrophage migration inhibitory factor; MIF; Oligomerization; Sedimentation equilibrium; Sedimentation velocity; Partial specific volume

1. Introduction

Macrophage migration inhibitory factor (MIF, also known as glycosylation inhibiting factor, GIF) is an interesting protein that has been reported to have multiple cytokine or hormone-like activities as well as enzymatic activities. There has been much conflicting information about the state of oligomerization of this protein in solution. Initially Blocki et al. purified rat MIF and reported it as a monomer based on size-exclusion chromatography (SEC) [1]. Then Nishihara and co-workers reported that rat MIF is a dimer based on SEC and sedimentation equilibrium [2,3]. A form of MIF from bovine brain was then reported as monomeric based on SEC [4], while another group reported human MIF is a trimer based on dynamic light scattering [5]. Subsequently a fourth group reported that human MIF chromatographs as a dimer on SEC, but concluded based on chemical cross-linking studies that both human and mouse MIF

*Corresponding author. Tel.: +1-805-388-1074; fax: +1-805-388-7252.
E-mail address: jphilo@mailway.com (J.S. Philo).

0301-4622/04/$ - see front matter © 2003 Elsevier B.V. All rights reserved.
doi:10.1016/j.bpc.2003.10.010

exist as a mixture of monomer, dimer and trimer, with monomer and dimer as the predominant species [6]. Moreover, they observed no change in oligomer distribution for protein concentrations from 1.2 to 220 μg/ml, implying that the presence of multiple oligomers is not due to weak association but rather that the different oligomeric forms are not in mass-action equilibrium. A fifth group reported mouse MIF runs as a dimer on SEC, but concluded it is a trimer based on their cross-linking approach [7].

In contrast to this conflicting solution data, all of the different groups that have obtained the structure of human or rat MIF by X-ray crystallography have shown MIF to be a trimer [8–11], including data for mutants [12], in the presence of small-molecule inhibitors [13,14], and that for a MIF homolog from a nematode [15]. One unusual feature of the trimer structure is a solvent-accessible central pore or channel. The trimer has an extensive inter-subunit interface, and each monomer has two short β-strands contributed by an adjacent subunit to further interlock the trimeric structure [11]. Given this solid structural evidence for a trimer, as well as the nature of the structure, it seems rather surprising that the solution data are so inconsistent. Consequently we have re-examined the solution mass, homogeneity and hydrodynamic properties of human MIF by sedimentation equilibrium and sedimentation velocity. These new sedimentation equilibrium studies encompass many samples covering a 100-fold range of loading concentrations and multiple rotor speeds, analyzed using modern global analysis methods, rather than the single concentration used in earlier studies [2,3]. The sedimentation velocity studies directly address the homogeneity of these samples, and the possible existence of oligomers that are not in reversible mass-action equilibrium with monomer or 'incompetent monomer' that is incapable of forming the trimeric structure seen in the crystals. The velocity data also for the first time directly define the hydrodynamic properties of GIF. Lastly, because the interpretation of analytical ultracentrifugation data requires knowledge of the protein's partial specific volume, $\bar{v}$, to provide the buoyancy correction, we have experimentally determined the $\bar{v}$ value for GIF via sedimentation equilibrium in D_2O/H_2O mixtures (the Edelstein and Schachman method) [16]. These studies have confirmed that MIF is indeed a tightly associated trimer in solution, but one with an unusual partial specific volume.

2. Materials and methods

2.1. Reagents

Recombinant human MIF (rhMIF) was cloned and expressed in *Escherichia coli* by the Molecular Biology Department at IDEC. The bacterial cell pellets were suspended in lysis buffer which contained 50 mM sodium acetate, pH 5.0, 40 mM $MgCl_2$ and 0.2 mg/ml DNase. The suspension was passed through a French press three times to lyse the cells. Lysate was centrifuged and the supernatant was saved and passed through a 0.45 μm filter for chromatography.

The initial separation was performed using a SP Sepharose (Pharmacia) cationic ion-exchange column eluted with a linear NaCl gradient in the elution buffer (50 mM sodium acetate, pH 5.0). Fractions containing rhMIF were pooled and concentrated by an Amicon concentrator with a DIAFLO ultrafiltration membrane YM3 (Millipore). The concentrated material was then loaded onto a Toso-Haas G3000SW gel filtration column that was equilibrated with 100 mM NaCl. The fractions containing rhMIF were collected and further concentrated. These purification procedures typically achieved more than 99% purity of the target protein. The N-terminal methionine was not present on the final product, as confirmed by mass spectrometry.

2.2. Sedimentation equilibrium

Sedimentation equilibrium experiments were done at 25 °C in a Beckman Optima XL-A analytical ultracentrifuge using 6-channel charcoal-epon centerpieces. Optical scans (absorbance vs. radius) were recorded at wavelengths of 280, 293 or 230 nm (depending on the concentration). Samples were spun for a period of 24 h at each rotor speed and the attainment of equilibrium confirmed by the absence of change for scans

taken 4 h apart. For the experiments in Dulbecco's phosphate buffered saline without calcium or magnesium (PBS) nine samples were loaded at initial concentrations of 10, 20, 40, 80, 160, 320, 480, 640 and 1070 μg/ml and run at rotor speeds of 18 000 and 24 000 rev./min. For the D_2O/H_2O studies 10 samples were run at a constant protein concentration of 315 μg/ml in 20-fold diluted PBS containing various proportions of H_2O or 99% D_2O (Aldrich) and also run at both 18 000 and 24 000 rev./min. At the end of each experiment the rotor was taken to 44 000 rev./min to pellet most of the sample and a scan recorded after 12–16 h to obtain an experimental baseline offset.

The resulting data were analyzed by global nonlinear least squares techniques using the program KDALTON [17,18]. For the D_2O/H_2O studies the data for each sample at both rotor speeds were jointly analyzed as a single ideal species. A solvent density of 1.00399 g/ml was assumed for PBS as we had measured previously [19]. A partial specific volume of 0.7351 ml/g for MIF at 25 °C, and the densities of the solvents containing D_2O, were calculated using the program SEDNTERP by Tom Laue and John Philo [20]. Protein concentrations reported here are based on a calculated $A_{280,1\ cm}$ of 0.979 [21].

2.3. Sedimentation velocity

Sedimentation velocity experiments were done at 20 °C using 2-channel charcoal-epon centerpieces (12 mm pathlength) and a rotor speed of 60 000 rev./min. Data were analyzed using the programs SVEDBERG version 6.39 by J. Philo [22] or the $c(s)$ method in SEDFIT version 6.0 by P. Schuck [23]. During the $c(s)$ analysis the frictional coefficient ratio was set to match that of the major component, which was assumed to be a MIF trimer. Hydrodynamic analysis was done using the Teller method as implemented in SEDNTERP [20].

2.4. Structure-based hydrodynamic modeling

Hydrodynamic bead modeling calculations were done using the highest resolution structure available, PDB file 1GD0 (1.5 Å resolution) [13] via the program HYDROPRO version 5 [24]. The residues from the His-tag sequence present on that MIF construct but absent from our protein were removed from the PDB file, as well as the ordered waters and ions. This calculation was done using the consensus $\bar{v}_{20°} = 0.7569$ ml/g (see Section 3.3 below) and the default atomic radius of 3.1 Å (which corresponds to typical hydration values).

3. Results and discussion

3.1. Sedimentation equilibrium in PBS

Sedimentation equilibrium experiments were done for nine samples of MIF in PBS spanning over a 100-fold range in loading concentration at two rotor speeds. These data show remarkably little variation in solution mass with concentration, as illustrated by the data at 18 000 rev./min for three of the samples which span a 28-fold range in loading concentration, as shown in Fig. 1. The apparent mass of ~33 kDa is well above the dimer mass of 24.690 kDa, supporting the existence of trimers as seen in the crystal structures, but the mass is also significantly below the full trimer mass of 37.035 kDa.

As might be expected from the graphical analysis, if we assume all samples contain only a single, ideal species this results in a fairly good global fit to all 18 data sets (9 concentrations, 2 rotor speeds) returning a weight-average mass of 33.38 kDa with a statistical 95% confidence region of 33.17–33.60 kDa. If we instead divide the data sets into high, middle and low concentration groups and analyze each group separately as a single ideal species, the masses are 33.12 kDa, 34.03 kDa and 33.00 kDa, respectively. The small drop in mass from the middle to low concentration group suggests there may be a small amount of dissociation at the lowest concentrations. However, if dissociation were the reason the low concentration data gives a mass below that of trimer, one would expect the mass for the high concentration data to increase significantly and approach that of trimer.

The fact that the apparent mass actually drops slightly as we go from the middle group to higher concentration suggests that we are seeing some

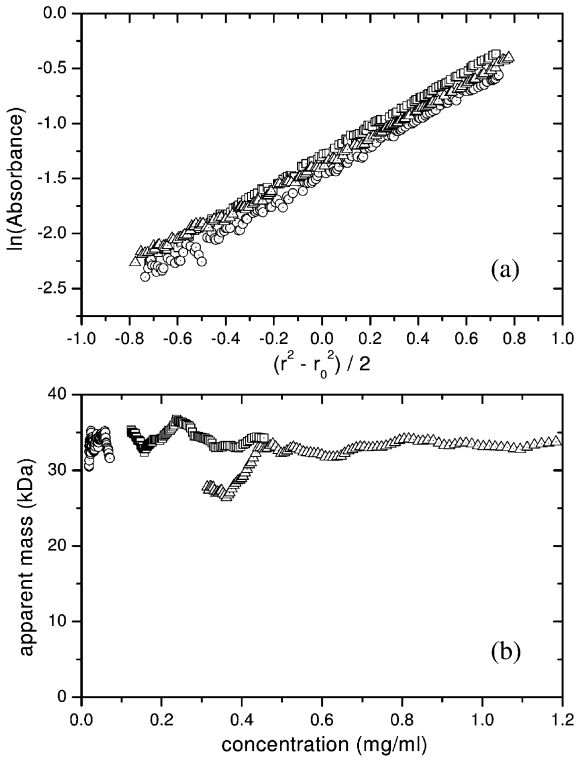

Fig. 1. Sedimentation equilibrium data at 18 000 rev./min for three samples initially loaded at ~1.08 mg/ml (diamonds, scanned at 293 nm), 315 μg/ml (squares, scanned at 280 nm) and 39 μg/ml (circles, scanned at 230 nm). Panel A is a $\ln(c)$ vs. $r^2/2$ plot, in which a single species gives a straight line with a slope proportional to buoyant mass. In panel B these data are plotted as apparent mass vs. concentration, with apparent mass determined from the slopes in panel A. Each point in panel B is determined from the slope of 40 adjacent points in A, with the corresponding concentration determined from the average for those 40 points; the group of 40 moves along the data one point at a time.

solution non-ideality ('molecular crowding') effects that reduce the apparent mass as the concentration increases, which is not unexpected at concentrations in the 1 mg/ml range or higher. Indeed, if we account for solution non-ideality by allowing a non-zero second virial coefficient, we get a slightly better single-species fit, returning a best-fit mass of 33.53 [33.25–33.82] kDa and a second virial coefficient of 8.4 [−6.0 to 23]$\times 10^{-5}$ ml mol/g^2, a value in excellent agreement with the predicted simple excluded-volume effects for a spherical molecule, $4\bar{v}/\mathrm{M} = 8.8\times 10^{-5}$ ml mol/g^2. This fit and its associated residual plot (deviations between the data and the fit) is shown in Fig. 2.

The next step is to try fitting these data to reversible self-association models. Given the evidence for trimers, the simplest such model is a monomer–trimer model ($3\mathrm{A} \leftrightarrow \mathrm{A}_3$) with a dissociation constant defined by

$$K = \frac{[A]^3}{[A_3]}$$

In fitting to association models one key choice is whether to fix the monomer mass at the known sequence value or to allow it to vary as a fitting parameter. Generally one prefers to fix the value at the sequence value, both because this makes scientific sense and because it reduces the number of fitting variables and thereby increases the reliability and precision of the dissociation constant. However, in this case if we fix the monomer mass at the sequence value we get a quite unsatisfactory fit: the overall variance is more than twice that for a single-species fit, and the deviations between the residuals are systematically positive or negative over large regions of each sample rather than randomly distributed about a mean deviation of zero (not shown). This fit returns $K = 1.2\times 10^{-5}$ (mg/ml)^2, i.e. an association weak enough to give a few percent monomer even at concentrations of 1 mg/ml. A monomer–dimer–trimer fit using a fixed monomer mass was also quite unsatisfactory (and for a closed ring-like trimer as seen in the crystal structures significant amounts of dimer would not be expected from energetic considerations).

If we instead allow the monomer mass to vary during a monomer–trimer fit we get a good fit (but one not significantly better than the single-species fit). That fit returns a monomer mass of 11.232 kDa [11.156–11.310] and $K = 4\times 10^{-8}$ (mg/ml)^2 [5×10^{-9}–1.6×10^{-7}]. It is important to remember that the quantity directly measured in sedimentation equilibrium is the buoyant mass, M_b, given by $M_b = M(1-\bar{v}\rho)$, where M is the true mass, $\bar{v}$ is the protein's partial specific volume,

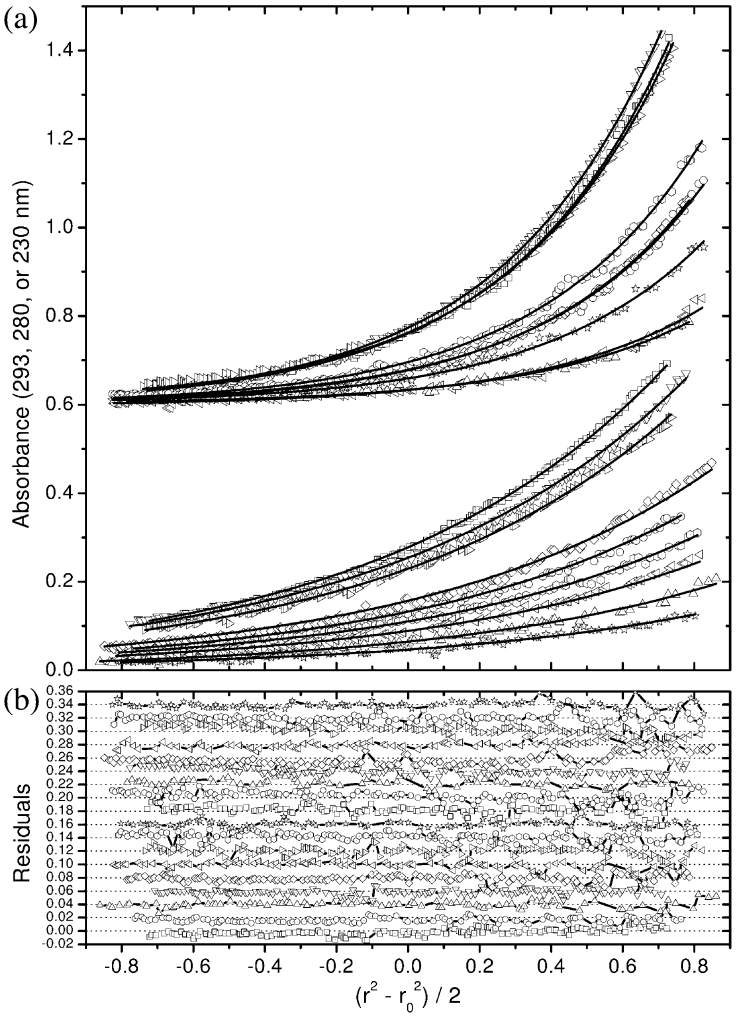

Fig. 2. (Panel A) Overlay of data (points) and fitted curves (lines) for a global analysis of 18 data sets for MIF in PBS analyzed as a single non-ideal species of mass 33.53 kDa and second virial coefficient of 2.8×10^{-3} ml/mg. To reduce data overlap the data sets at 24 000 rev./min have been shifted vertically by 0.6 AU. (Panel B) Residuals for the fit shown in panel A; successive data sets have been offset by 0.02 AU for clarity.

and ρ is the solvent density. Thus since the true monomer mass is known, in this model we are essentially allowing the partial specific volume to vary from the nominal value based on amino acid composition. Viewed in that way, the best fit corresponds to $\bar{v}_{25°}=0.7587$ ml/g [0.7570–0.7602] rather than the expected value of 0.7351 ml/g.

Another possible explanation for the lack of concentration dependence but an average mass intermediate between dimer and tetramer would be that we have a mixture of oligomers that are not in mass-action equilibrium. Our samples might, for example, contain some so-called ‘incompetent monomer’, a partially-denatured form that is not capable of normal self-association. Typically when mixtures are analyzed by sedimentation equilibrium the apparent mass drops significantly with increasing rotor speed. This arises because the higher mass species become more enriched at the

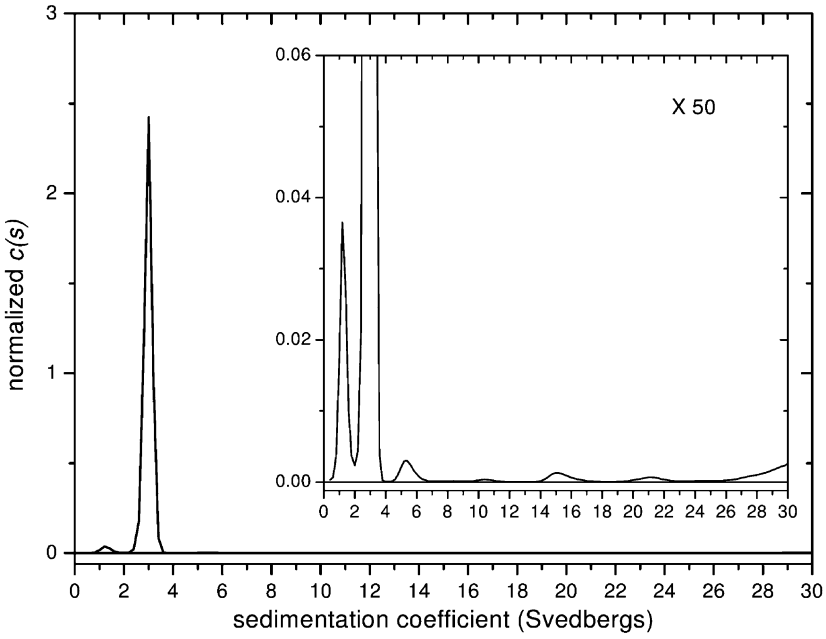

Fig. 3. Sedimentation coefficient distribution for MIF in PBS. The inset has the vertical scale expanded 50-fold so that the minor components can be seen. The distribution is normalized so the total area under the curve is 1.0, and thus the area of each peak gives the fraction of that species.

very base of the cell, but that region cannot be used in the analysis because of optical artifacts that arise there, so the higher mass species become increasing 'lost' from the analysis at high rotor speeds. In this case, however, analyzing the two rotor speeds separately as a single non-ideal species gives masses of 33.66 and 33.40 kDa at 18 000 rev./min and 24 000 rev./min, respectively, a difference that is not statistically significant.

Thus overall these sedimentation equilibrium experiments seem to indicate that these samples are predominantly trimer, but it is not entirely clear whether the apparent mass falls below the expected value for trimer because MIF has an unusual partial specific volume or perhaps whether these samples are a non-equilibrating mixture of different oligomers. In order to more directly address the possibility of a mixture, we have also done sedimentation velocity experiments.

3.2. Sedimentation velocity

Sedimentation velocity is better than sedimentation equilibrium at analyzing mixtures as a consequence of the stronger physical separation at high rotor speeds. Fig. 3 shows the sedimentation coefficient distribution for a sample of MIF in PBS loaded at 65 μg/ml, obtained by Peter Schuck's high resolution $c(s)$ method [23]. This result indicates the sample is fairly homogeneous, with the major peak at 3.0 S representing 96.7% of the total absorbance. A minor peak at 1.2 S represents only 2.0% of the total, and the balance of 1.3% is distributed among traces of various species at 5 S and above, which presumably represent aggregates.

What species do the 1.2 S and 3 S components represent? Analysis of these data as a mixture of 3 independently-sedimenting components (with the third component representing an average of the trace fast sedimenting species) using the program SVEDBERG [22] gives a good fit of the data. This fit indicates that the major component (97.4% of the total) has $s=2.979$ S [95% confidence 2.977–2.981] and $D=8.22\times10^{-7}$ cm^2/s [8.18–8.28]. The ratio of those values implies a buoyant mass of 8.832 kDa [8.764–8.881], which at $\bar{v}=$

0.7330 ml/g calculated at 20 °C corresponds to a true mass of 33.56 [33.30–33.75] kDa, reasonably consistent with assignment of this species as a trimer. The slowly sedimenting component (1.4% of the total) has $s=1.39$ S [1.35–1.42] and $D=7.4\times10^{-7}$ cm^2/s [5.3–10.3], corresponding to $M_b=4.6$ kDa [3.0–5.9] or a true mass of 17 [11–23] kDa. This suggests that this latter species is a monomer not in rapid equilibrium with the trimer species, i.e. an incompetent monomer. Given the multiple reports that MIF is predominantly a dimer [2,3], or a mixture of species including dimer [6], it is worth noting that these velocity studies did not detect any dimer.

These sedimentation velocity results are quite consistent with the sedimentation equilibrium data, suggesting that the vast majority of the sample has an apparent mass of ~33.5 kDa. Although there may be 1–2% of an incompetent monomer species present, that amount is far too little to account for the average mass from sedimentation equilibrium being ~9% below the expected value for a trimer. Thus we are left with the puzzle of why the apparent mass is too low. Could our calculated partial specific volume be significantly in error? To address that possibility we decided to carry out further sedimentation equilibrium studies in D_2O/H_2O mixtures in order to obtain an experimental value for $\bar{v}$.

3.3. Sedimentation equilibrium in D_2O/H_2O mixtures

The Edelstein and Schachman method [16] involves a series of sedimentation equilibrium experiments where the solvent density is systematically varied over as wide a range as possible. Since $M_b=M(1-\bar{v}\rho)$, by assuming that the protein's weight-average mass is independent of solvent density, the measured buoyant mass becomes a linear function of solvent density, and one can extract both $\bar{v}$ and the true M from the slope and intercept of a plot of buoyant mass vs. density. When solvent density is altered by adding D_2O additional corrections are made to account for the change in protein mass from proton/deuteron exchange [16]. Ten samples in 20-fold diluted PBS at 0–89.1% D_2O were measured at two rotor speeds, giving the data shown in Fig. 4. Extrapolation of the best-fit line through these data back to the origin, as shown in Fig. 4b, gives a true mass of 39.06 ± 0.96 kDa, confirming that the predominant species is indeed trimer, while the slope of this line implies that that the partial specific volume at 25 °C is 0.765 ± 0.17 ml/g rather than the calculated value of 0.735 ml/g. Thus the apparent miss-match between the expected trimer mass and the masses reported above from both sedimentation equilibrium and sedimentation velocity seems to arise because this protein has an unusually large partial specific volume. If we revise $\bar{v}$ to 0.765 ml/g the mass estimate from the fit shown in Fig. 2 becomes $M=37.9\pm2.8$ kDa (with the uncertainty arising predominantly from that in $\bar{v}$), a value which is quite consistent with this material being 97–98% trimer plus traces of monomer and higher mass aggregates, as indicated by the sedimentation velocity data.

Although the D_2O/H_2O experiments have confirmed our suspicion that the calculated $\bar{v}$ appears to be significantly too low, the limited range of solvent densities that can be obtained via this approach still leaves us with a fairly large uncertainty in $\bar{v}$. Can we use our knowledge of the sequence mass to refine $\bar{v}$? If we now assign the mass of the major species in the velocity data at the trimer sequence mass, the buoyant mass from the SVEDBERG analysis can be used to estimate $\bar{v}$, which gives $\bar{v}=0.7576$ ml/g [0.7562–0.7594] at 20°, implying 0.7597 ml/g [0.7583–0.7615] at 25°. Recall also that our earlier fit of the sedimentation equilibrium data in PBS to a reversible monomer–trimer model was consistent with the monomer sequence mass if $\bar{v}_{25°}=0.7587$ ml/g [0.7570–0.7602]. Thus all the data are consistent with a 'best' or 'consensus' value for $\bar{v}_{25°}$ of 0.759 ml/g (or $\bar{v}_{20°}=0.7569$) with an uncertainty of approximately ±0.003 ml/g.

3.4. Hydrodynamic results

With $\bar{v}$ and the mass assignments now clarified, we can correct the sedimentation velocity results to standard conditions and do further hydrodynamic analysis. Those results for trimer and monomer are summarized in Table 1. The 2.55 nm hydro-

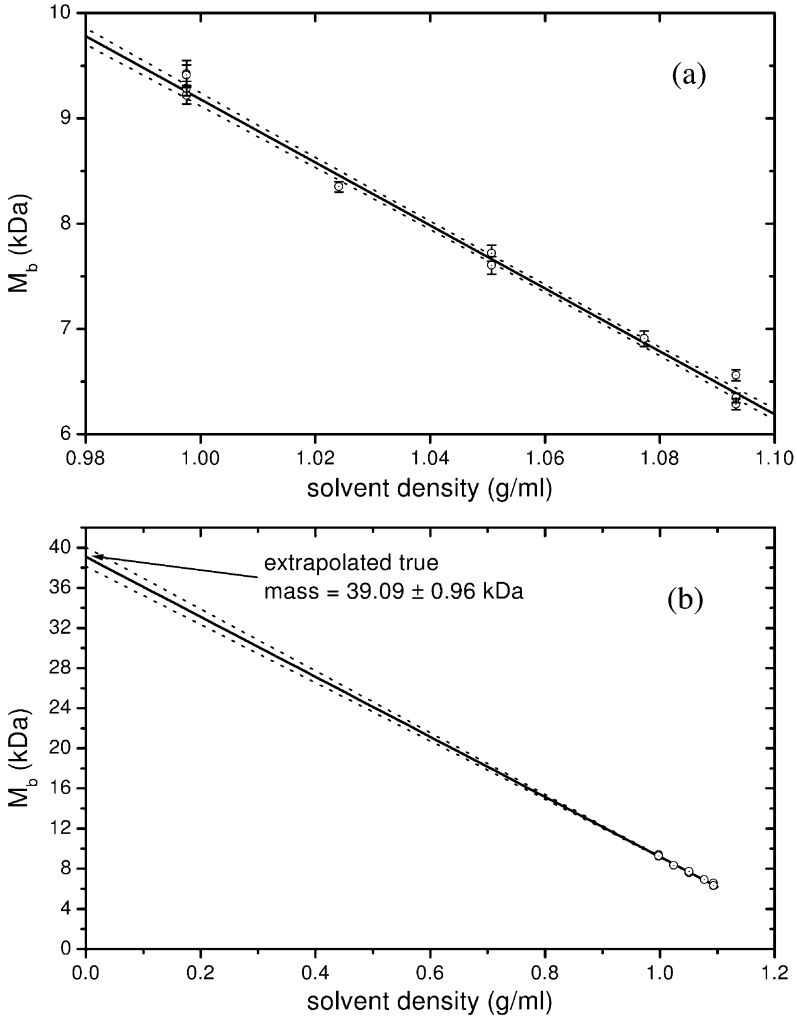

Fig. 4. Variation in buoyant mass of MIF from sedimentation equilibrium with solvent density (varied by using D_2O/H_2O mixtures). The solid line is the best-fit line through the data (fitted with data weighted according to the error estimates for each sample); the dotted lines indicate the 1σ confidence band. The slope of this line gives the product $-M\bar{v}$. The lower panel shows the extrapolation to $\rho=0$ to obtain the true mass, M.

dynamic radius we obtain for the MIF trimer is in good agreement with the 2.6–2.8 nm value reported for MIF from dynamic light scattering [5]. As expected from the fairly compact and symmetric structures seen by X-ray crystallography, the MIF trimer has a fairly low frictional coefficient ratio of 1.14 relative to that of an anhydrous sphere. If analyzed as either an oblate or prolate ellipsoid, and using a hydration of 0.345 g/g as estimated by the Kuntz method [25], this would indicate an axial ratio of $\sim$1.24, somewhat more asymmetry than is apparent by eye from the X-ray structure. However, a detailed calculation of the sedimentation coefficient from the X-ray coordinates using bead modeling predicts a sedimentation coefficient of 3.05 S, only 1.5% lower than our experimental value. Thus the X-ray structure of the trimer is quite consistent with our hydrodynamic data.

Table 1
Summary of hydrodynamic results

	Trimer (using consensus experimental $\bar{v}_{25°}=0.759$ ml/g)	Monomer (using consensus experimental $\bar{v}_{25°}=0.759$ ml/g)	Monomer (using calculated $\bar{v}_{25°}=0.735$ ml/g)
$s_{20,w}$	3.096 ± 0.002 S	1.442 ± 0.03 S	1.438 ± 0.03 S
$D^{a}_{20,w}$	8.34×10^{-7} cm^2/s	1.16×10^{-6} cm^2/s	1.06×10^{-6} cm^2/s
Hydrodynamic radius, R_h	2.55 nm	1.82 nm	2.03 nm
Frictional ratio, f/f_0	1.14	1.17	1.30
$s_{20,w}$ calculated from X-ray structure[b]	3.05 S	1.33 S	1.45 S

[a]Calculated from the sequence mass and the sedimentation coefficient; [b]from bead modeling using HYDROPRO; see *Methods* for details.

It is unclear whether the monomer will have the same unusual $\bar{v}$ as the trimer or the more normal calculated value, so we have shown its experimental hydrodynamic parameters in Table 1 using both assumptions. It is expected that the monomer f/f_0 ratio will be significantly higher than that for trimer, particularly because this appears to be a partially-denatured 'incompetent' monomer. We have also calculated a theoretical sedimentation coefficient for the monomer based on a single subunit within the trimer X-ray structure, i.e. assuming no structural change upon dissociation. Even if the monomer is not in a partially-denatured state, it seems likely that it would be less hydrodynamically compact than a subunit of the trimer. In particular, the first three β strands at the amino terminus are unlikely to maintain the same conformation in the monomer, and may well be disordered, since they normally form a 'finger' wrapping around the adjacent subunit within the trimer, and two of them actually form extensions of β sheets within the adjacent subunit. Therefore this bead model calculation should represent the maximum possible $s_{20,w}$ for monomer. However, the calculated monomer $s_{20,w}$ is 1.33 S, below the experimental value, if we assume the monomer $\bar{v}$ is the same as our 'consensus' value for trimer, $\bar{v}_{25°}=0.759$ ml/g. If, however, the monomer has the calculated $\bar{v}$, the predicted $s_{20,w}$ becomes 1.45 S, in agreement with the experimental value. This latter agreement is probably coincidental rather than suggesting that the monomer truly retains the tertiary structure from the trimer; if that were true then it would surely not be incompetent for assembly into trimers, as the data proves. Rather, the main point of this hydrodynamic analysis is that it would be extremely hard to reconcile the rapid sedimentation of the monomer if it has the same abnormally high $\bar{v}$ as the trimer. Further, even if it has the 'normal' calculated $\bar{v}$ it still appears that the monomer conformation is more compact than would be expected, perhaps indicating that the amino-terminal 'finger' region has moved back toward the main body of the subunit to form a more compact structure.

3.5. Discussion

Our findings should certainly lay to rest any doubts MIF forms trimers under normal solution conditions as well as under conditions leading to crystallization. The fact that we see little dissociation of trimers at the lowest concentrations we can reach in the analytical centrifuge also shows the association is strong and specific. The fact that the velocity analysis indicates the presence of some incompetent monomer means that the trimer dissociation constant of 4×10^{-8} (mg/ml)^2 (or equivalently 7.7×10^{-16} M^2) obtained from the fit with variable monomer mass should be probably be viewed as an upper limit for the dissociation constant.

Why is the $\bar{v}$ of the MIF trimer unusually large? One effect known to significantly alter $\bar{v}$ values is preferential binding or exclusion of salts at the protein surface. However, we do not believe that

explanation applies here. Such effects are usually only significant at much higher salt concentrations than the physiological ionic strength employed for the bulk of our studies, and moreover the D_2O/H_2O experiments were deliberately done at much lower ionic strength to remove such a possibility. To understand why the calculated $\bar{v}$ value for a particular protein may be significantly in error, we first must understand how these calculations are done and why they are normally successful. The calculations simply assign a volume to each amino acid residue, assuming additivity of volumes, with the residue volumes usually assigned based on density data for amino acids or small peptides [26–28]. Such calculations therefore neglect (or at least oversimplify) two significant contributions to the $\bar{v}$ of real proteins: (1) the fact that water molecules bound at the protein surface have a different density than the bulk solvent; and (2) the fact that protein structures are typically not fully closely-packed and have internal cavities (voids). The effects of the protein on the density of the bound water are complex. The water in proximity to charged groups has a higher density than the bulk (electrostriction), but that near hydrophobic groups is thought to have a lower-density structure like ice. Overall the density of the bound water is usually thought to be significantly above that of bulk water [29]. Increases in volume of the interior of the protein over the expected residue volumes can include an increased average volume for residues near the surface [30] in addition to the presence of voids [31]. In typical proteins the surface hydration and interior volume effects are of about equal magnitude (approx. 0.02 ml/g) but with opposite sign, so they fortuitously approximately cancel.

Thus a $\bar{v}$ much higher than the calculated value might result from either an unusual amount or type of hydration, or an unusually large number or size of voids within the structure. The excellent match between the sedimentation coefficient of the trimer and the value calculated from the structure (which assumes typical hydration) argues against an unusual total amount of hydration. Further, a search for voids in MIF (PDB structure 1GD0) using the program CASTp [32] did not show anything unusual. It is therefore tempting to speculate that the abnormal $\bar{v}$ of MIF may be directly related to the central pore observed in the crystal structures. However, the only evidence we can provide to support that hypothesis is the indirect argument made above that the sedimentation coefficient of the monomer suggests it has a normal $\bar{v}$, and that observation actually does not even distinguish whether the large $\bar{v}$ is a consequence of the pore or a consequence of forming a trimer. Perhaps these new experimental results will stimulate a re-examination of the X-ray crystallography data and/or some molecular dynamics simulations that will shed further light on the underlying cause of this phenomenon.

Unfortunately these new results cannot completely reconcile the varied earlier reports of MIF's state of oligomerization. The reports of monomer or dimer based on SEC elution could easily be explained as errors due to the fairly compact structure of the trimer and/or delayed elution due to column interactions. Even our finding of an unusual $\bar{v}$ for MIF cannot, however, explain the reported mass of 23.6 kDa from sedimentation equilibrium [3], since revising $\bar{v}$ would only increase that mass by ~10%. A possible explanation for their results, as well as other findings of mixtures of different oligomers, is that some MIF preparations may contain a substantial amount of incompetent monomer.

References

[1] F.A. Blocki, P.M. Schlievert, L.P. Wackett, Rat liver protein linking chemical and immunological detoxification systems, Nature 360 (1992) 269–270.

[2] J. Nishihira, T. Kuriyama, H. Nishino, T. Ishibashi, M. Sakai, S. Nishi, Purification and characterization of human macrophage migration inhibitory factor: evidence for specific binding to glutathione and formation of subunit structure, Biochem. Mol. Biol. Int. 31 (1993) 841–850.

[3] J. Nishihira, T. Kuriyama, M. Sakai, S. Nishi, S. Ohki, K. Hikichi, The structure and physicochemical properties of rat liver macrophage migration inhibitory factor, Biochim. Biophys. Acta 1247 (1995) 159–162.

[4] A. Galat, S. Riviere, F. Bouet, A. Menez, A diversified family of 12-kDa proteins with a high amino acid sequence similarity to macrophage migration-inhibitory factor (MIF), Eur. J. Biochem. 224 (1994) 417–421.

[5] H.W. Sun, M. Swope, C. Cinquina, S. Bedarkar, J. Bernhagen, R. Bucala, et al., The subunit structure of

human macrophage migration inhibitory factor: evidence for a trimer, Protein Eng. 9 (1996) 631–635.
[6] R. Mischke, R. Kleemann, H. Brunner, J. Bernhagen, Cross-linking and mutational analysis of the oligomerization state of the cytokine macrophage migration inhibitory factor (MIF), FEBS Lett. 427 (1998) 85–90.
[7] K. Bendrat, Y. Al Abed, D.J. Callaway, T. Peng, T. Calandra, C.N. Metz, et al., Biochemical and mutational investigations of the enzymatic activity of macrophage migration inhibitory factor, Biochemistry 36 (1997) 15 356–15 362.
[8] H. Sugimoto, M. Suzuki, A. Nakagawa, I. Tanaka, J. Nishihira, Crystal structure of macrophage migration inhibitory factor from human lymphocyte at 2.1 A resolution, FEBS Lett. 389 (1996) 145–148.
[9] M. Suzuki, H. Sugimoto, A. Nakagawa, I. Tanaka, J. Nishihira, M. Sakai, Crystal structure of the macrophage migration inhibitory factor from rat liver, Nat. Struct. Biol. 3 (1996) 259–266.
[10] Y. Kato, T. Muto, T. Tomura, H. Tsumura, H. Watarai, T. Mikayama, et al., The crystal structure of human glycosylation-inhibiting factor is a trimeric barrel with three 6-stranded beta-sheets, Proc. Natl. Acad. Sci. USA 93 (1996) 3007–3010.
[11] H.W. Sun, J. Bernhagen, R. Bucala, E. Lolis, Crystal structure at 2.6-A resolution of human macrophage migration inhibitory factor, Proc. Natl. Acad. Sci. USA 93 (1996) 5191–5196.
[12] S.L. Stamps, A.B. Taylor, S.C. Wang, M.L. Hackert, C.P. Whitman, Mechanism of the phenylpyruvate tautomerase activity of macrophage migration inhibitory factor: properties of the P1G, P1A, Y95F and N97A mutants, Biochemistry 39 (2000) 9671–9678.
[13] M. Orita, S. Yamamoto, N. Katayama, M. Aoki, K. Takayama, Y. Yamagiwa, et al., Coumarin and chromen-4-one analogues as tautomerase inhibitors of macrophage migration inhibitory factor: discovery and X-ray crystallography, J. Med. Chem. 44 (2001) 540–547.
[14] A.B. Taylor, W.H. Johnson Jr, R.M. Czerwinski, H.S. Li, M.L. Hackert, C.P. Whitman, Crystal structure of macrophage migration inhibitory factor complexed with (E)-2-fluoro-p-hydroxycinnamate at 1.8 A resolution: implications for enzymatic catalysis and inhibition, Biochemistry 38 (1999) 7444–7452.
[15] T.H. Tan, S.A. Edgerton, R. Kumari, M.S. McAlister, S.M. Roe, S. Nagl, et al., Macrophage migration inhibitory factor of the parasitic nematode *Trichinella spiralis*, Biochem. J. 357 (2001) 373–383.
[16] S.J. Edelstein, H.K. Schachman, The simultaneous determination of partial specific volumes and molecular weights with microgram quantities, J. Biol. Chem. 242 (1967) 306–311.
[17] J.S. Philo, J. Talvenheimo, J. Wen, R. Rosenfeld, A.A. Welcher, T. Arakawa, Interactions of neurotrophin-3 (NT-3), brain-derived neurotrophic factor (BDNF), and the NT-3/BDNF heterodimer with the extracellular domains of the TrkB and TrkC receptors, J. Biol. Chem. 269 (1994) 27 840–27 846.
[18] J.S. Philo, Improving sedimentation equilibrium analysis of mixed associations using numerical constraints to impose mass or signal conservation, Methods Enzymol. 321 (2000) 100–120.
[19] J.S. Philo, K.H. Aoki, T. Arakawa, L.O. Narhi, J. Wen, Dimerization of the extracellular domain of the erythropoietin (EPO) receptor by EPO: one high-affinity and one low-affinity interaction, Biochemistry 35 (1996) 1681–1691.
[20] T.M. Laue, B.D. Shah, T.M. Ridgeway, S.L. Pelletier, Computer-aided interpretation of analytical sedimentation data for proteins, in: S.E. Harding, A.J. Rowe, J.C. Horton (Eds.), Analytical Ultracentrifugation in Biochemistry and Polymer Science, Royal Society of Chemistry, Cambridge, 1992, pp. 90–125.
[21] H. Edelhoch, Spectroscopic determination of tryptophan and tyrosine in proteins, Biochemistry 6 (1967) 1948–1954.
[22] J.S. Philo, An improved function for fitting sedimentation velocity data for low-molecular-weight solutes, Biophys. J. 72 (1997) 435–444.
[23] P. Schuck, Size-distribution analysis of macromolecules by sedimentation velocity ultracentrifugation and Lamm equation modeling, Biophys. J. 78 (2000) 1606–1619.
[24] J.G. de la Torre, M.L. Huertas, B. Carrasco, Calculation of hydrodynamic properties of globular proteins from their atomic-level structure, Biophys. J. 78 (2000) 719–730.
[25] I.D. Kuntz Jr, T.S. Brassfield, Hydration of macromolecules. II. Effects of urea on protein hydration, Arch. Biochem. Biophys. 142 (1971) 660–664.
[26] A.A. Zamyatnin, Amino acid, peptide and protein volume in solution, Annu. Rev. Biophys. Bioeng. 13 (1984) 145–165.
[27] E.J. Cohn, J.T. Edsall, Proteins, Amino Acids and Peptides, Reinhold, New York, 1943.
[28] S.J. Perkins, Protein volumes and hydration effects. The calculations of partial specific volumes, neutron scattering matchpoints and 280-nm absorption coefficients for proteins and glycoproteins from amino acid sequences, Eur. J. Biochem. 157 (1986) 169–180.
[29] D.I. Svergun, S. Richard, M.H. Koch, Z. Sayers, S. Kuprin, G. Zaccai, Protein hydration in solution: experimental observation by X-ray and neutron scattering, Proc. Natl. Acad. Sci. USA 95 (1998) 2267–2272.
[30] M. Gerstein, C. Chothia, Packing at the protein–water interface, Proc. Natl. Acad. Sci. USA 93 (1996) 10 167–10 172.
[31] K.J. Frye, C.A. Royer, Probing the contribution of internal cavities to the volume change of protein unfolding under pressure, Protein Sci. 7 (1998) 2217–2222.
[32] J. Liang, H. Edelsbrunner, C. Woodward, Anatomy of protein pockets and cavities: measurement of binding site geometry and implications for ligand design, Protein Sci. 7 (1998) 1884–1897.